AUV TERRAIN RELATIVE NAVIGATION USING COARSE MAPS

Deborah K. Meduna[1]   **Stephen M. Rock**[1,2]   **Robert S. McEwen**[2]

dmeduna@stanford.edu   rock@stanford.edu   rob@mbari.org

[1] Dept. of Aeronautics and Astronautics
Stanford University, 496 Lomita Mall
Stanford, CA 94305

[2] Monterey Bay Aquarium Research Institute
7700 Sandholdt Road
Moss Landing, CA 95039

Abstract

Terrain Relative Navigation (TRN) provides an enabling technology for drift-free, low-cost navigation on many existing underwater vehicles. While high-performance TRN systems have been demonstrated using high-quality sensors and terrain maps, these systems can be very costly and the high-resolution bathymetry maps used are of limited availability. To extend the applicability of TRN, the authors previously addressed the performance trades in utilizing lower-cost, lower-accuracy sensor systems for terrain navigation. The current paper addresses the additional extension of TRN to coarse, ship-based maps which are more widely available. Performance studies assessing TRN performance over varying map resolution are presented for two sets of real-time field trials, performed over different terrains in Monterey Bay, CA. A posterior Cramér-Rao bound analysis provides insight into the terrain characteristics most relevant to the observed TRN performance reduction over coarser maps. Finally, the results from these studies are validated against 20m ship-based bathymetry maps. In these studies, moving from a 1m to a 30m resolution map is observed to reduce TRN estimation accuracy by a factor of only 2-3, resulting in sub-map resolution accuracies. The presented results indicate that, for the range of resolutions considered, coarse ship-based maps can potentially be utilized in place of higher-resolution AUV-based maps with only mild performance losses.

1 Introduction

Terrain relative navigation can enable drift-free, low-cost navigation for underwater vehicles, providing a powerful alternative to other underwater navigation methods including periodic resurfacing for GPS, dead-reckoning with high-accuracy inertial sensors, and/or deploying transponder arrays. TRN generates vehicle position estimates by matching terrain measurements against a stored terrain map. The technology was initially developed with TERCOM (Terrain Contour Matching) for cruise missile navigation, consisting of batch correlation of altimeter measurements [1].

Since TERCOM, numerous variants of TRN have been successfully developed for a range of platforms, including underwater vehicles [2], [3], [4], [5], [6], [7], [8], [9]. Many of these implementations report high accuracy performance by using a combination of high-quality instrumentation and high-accuracy Digital Elevation Model (DEM) terrain maps. Nygren, for example, demonstrated high performance through TERCOM-style batch correlation of large sonar measurement patches, created from combining several multibeam sonar pings with well-known relative spacing [3].

In [8], the authors demonstrated meter-level accuracy in field trials on the Monterey Bay Aquarium Research Institute (MBARI) mapping AUV, using either an Altimeter or Doppler Velocity Log (DVL) sonar measurements for correlations against a high-resolution (1 meter) DEM map. The presented results were aimed at evaluating the affect on TRN performance of using lower-cost, lower-accuracy vehicle instrumentation. Enabling TRN on these lower-cost sensor systems significantly expands the range of potential TRN applications.

This paper continues this work by addressing the additional concern of the performance effects in transitioning to coarser resolution terrain maps. Enabling effective TRN over low-accuracy terrain maps can substantially increase its applicability. For example, while DEM maps are available for much of Monterey Bay, California, only a small percentage have been generated with meter-level accuracy (e.g. by MBARI's mapping AUV). The vast majority of available DEM maps are derived

from ship-based bathymetry, resulting in resolutions on the order of 10's of meters.

Utilizing coarser resolution maps for terrain navigation, however, introduces important performance trade offs that have not been thoroughly addressed in AUV navigation literature [10]. The achievable accuracy of a TRN system is expected to be inversely related to the coarseness of the utilized terrain map. However, the rate of performance degradation and its dependence on underlying terrain properties is not well understood.

This paper explores the performance trades involved in moving to coarse DEM maps for TRN through case studies on two sets of real-time field trials, performed over different terrains in Monterey Bay, CA. A TRN configuration is presented which utilizes DVL sonar for terrain correlation and a point mass filter for estimate propagation. Empirical studies are presented using DEMs created at varying resolutions to assess TRN performance over coarser maps.

Reduced map resolution is observed to effect TRN performance through both decreased accuracy of the modeled terrain elevations, and a decreased ability of the map to represent the true terrain gradient variability. An analytical performance study based on the posterior Cramér-Rao bound is presented which provides a means for quantifying these effects for a given terrain. Finally, the results of these studies are validated against TRN performance with 20m ship-based bathymetry maps. The presented investigation shows that the TRN performance degrades gradually with decreased map resolution, implying that coarse ship-based maps on the order of 10s of meters can be effectively used for TRN without significant performance losses.

2 TRN Filter Implementation

The performance analysis and field trials presented in this paper are generated using a point mass filter TRN algorithm similar to that described in [8]. The terrain navigation system is modeled by the equation pair:

$$x_t = x_{t-1} + u_t + r_t \qquad (1)$$
$$y_t = h(x_t) + e_t \qquad (2)$$

with vehicle state given by:

$$x_t = [x_t^{North} \, x_t^{East}]^T. \qquad (3)$$

Equation 1 models the state propagation, where u_t is the change in vehicle state measured by an inertial navigation unit, and $r_t \sim N(0, \Sigma_r)$ is the process noise determined by the inertial drift rate and distance traveled. The sonar measurement is modeled by Equation

2, where $y_t \in \mathcal{R}^N$ is the N projected sonar measurements of terrain depth, $h(x_t)$ is the corresponding terrain depth at the sonar projected beam locations relative to state x_t, and $e_t \sim N(0, \Sigma_e)$ is the sonar measurement noise, modeled as 4% of the measured range.

Unfortunately, the true terrain surface in the measurement equation, $h(x_t)$, is not generally known. Instead, the terrain surface must be approximated by a model. In the geoscience community, the most common such terrain model is the DEM. A typical DEM represents the terrain by a grid of elevation values, uniformly distributed in North and East. The resulting model for terrain depth at any given location, $h(x_t)$, is given by Equation 4:

$$h(x_t) = \hat{h}(x_t) + v_t + \delta z \qquad (4)$$

where $\hat{h}(x_t)$ is the DEM estimated terrain depth at location x_t, v_t is the associated DEM modeling error, and δz is a depth bias term which accounts for variation in tide levels between the time of the DEM creation and the current vehicle mission.

In order to estimate terrain depth at any inter-grid location, a linear interpolation method is utilized:

$$\hat{h}_i(x_t) = \sum_{j=1}^{n} \lambda_j h_{i,j}^M[x_t] \qquad (5)$$

where $h_{i,j}^M[x_t]$ is the DEM value at the jth grid cell in the neighborhood of measurement $y_{t,i}$, and λ_j is the associated interpolation weight. Many interpolation methods can be represented as in Equation 5, including nearest-neighbor, bilinear, and bicubic. Each of these were evaluated for the current filter implementation and it was found that while bicubic interpolation performed the best, bilinear interpolation provided a better performance versus speed trade-off and was thus selected for the current filter. The tendency of higher order interpolation methods to give small performance gains at the expense of large computational effort has also been noted by several in the geoscience community [11], [12].

Using this interpolation method for terrain depth estimation results in the new measurement equation,

$$y_{t,i} = \lambda^T h_i^M[x_t] + \delta z + v_{t,i} + e_{t,i}. \qquad (6)$$

For simplicity, the DEM modeling error has been approximated as a zero-mean guassian, $v_t \sim N(0, \text{diag}(\sigma_v^2))$, where the covariance is given by:

$$\begin{aligned} \sigma_{v,i}^2 &= \lambda^T \text{Cov}(h^M, (h^M)^T)\lambda \qquad (7)\\ &= \lambda^T \sigma^2(h^M) + \lambda^T \left[A - \gamma(h^M, (h^M)^T) \right] \lambda \end{aligned}$$

where $A_{ij} = 0.5(h_i^M - h_j^M)^2$, and γ_{ij} is the variogram of the distance between grid points h_i^M and h_j^M. A variogram describes the expected mean square difference

between points at a specified spatial separation, and are fundamental to the field of geostatistics, initially developed by [13]. They are commonly used as a convenient means of inferring spatial covariance [14]. In the current implementation, a fractal variogram model is utilized, given by Equation 8:

$$\begin{aligned}
\gamma(s) &= 0.5E[((h(x) - h(x+s))^2] \\
&= a||s||^{2(3-D)}
\end{aligned} \tag{8}$$

where s is a separation (lag) distance between data points, and D is the fractal dimension, related to terrain roughness. Fractal models, initially developed by [15], are commonly used for representing variability in natural terrains.

Assuming that the sonar measurement noise is uncorrelated with the map error and errors between beams are independent, the probability of acquiring the current sonar measurement, y_t, given vehicle state x_t and depth bias δz is given by:

$$p(y_t|x_t, \delta z) = \alpha \exp\left(-\frac{1}{2}\sum_{i=0}^{N} w_i \left[y_{i,t} - \hat{h}_i(x_t) - \delta z\right]^2\right) \tag{9}$$

where

$$w_i = \frac{1}{\sigma_{e,i}^2 + \sigma_{v,i}^2}. \tag{10}$$

The resulting likelihood distribution is thus a three-dimensional function over x_t and δz. However, the depth bias term, which represents the depth offset due to tidal variations, is simply the offset between the map depth and the true vehicle depth plus altitude. As a result, δz is deterministic given the true vehicle position. Thus, the three-dimensional probability in Equation 9 can be approximated as a two-dimensional surface by replacing the depth bias term with its maximum likelihood estimate, given in Equation 11. This approximation is exact for a single time step.

$$\begin{aligned}
\delta\hat{z}(x_t) &= \frac{1}{\sum_i w_i}\sum_i w_i(y_{i,t} - \hat{h}_i(x_t)) \\
&= \eta w^T(y_t - \hat{h}(x_t))
\end{aligned} \tag{11}$$

The effect of this resulting depth bias term is to constrain the search to the sonar-measured altitude above the map and apply contour matching rather than depth profile matching. Both [3] and [4] use a similar contour-matching based TRN algorithm. The resulting two-dimensional likelihood of making measurement y_t at lo-

cation x_t is given by Equation 12:

$$p(y_t|x_t) = \alpha \exp\left(-\frac{1}{2}\sum_{i=0}^{N} w_i \left[\Pi(y_t - \hat{h}(x_t))\right]_i^2\right) \tag{12}$$

where

$$\Pi = I_N - \eta u w^T. \tag{13}$$

The likelihood surface is clearly highly nonlinear in the state, primarily due to the natural nonlinearity of the terrain function, $\hat{h}(x)$. This nonlinearity has been widely noted for terrain navigation filter applications, and increases with fewer measurement beams. As a result, a full Bayesian, non-parametric filter is needed for successful tracking of the vehicle state estimate. In this work, a point mass filter (PMF), or histogram filter, is utilized for state propagation. For low-dimensional search, the PMF is advantageous over other non-parametric filters, such as a particle filter, due to its higher robustness [4] and efficient indexing of DEM values. The PMF filter equations are given by:

$$\begin{aligned}
\tilde{p}(x_t) &= \sum_x p(x_t|x_{t-1}, u_t)p(x_{t-1}) &\tag{14} \\
p(x_t) &= \alpha p(y_t|x_t)\tilde{p}(x_t) &\tag{15}
\end{aligned}$$

where $p(x_t|x_{t-1}, u_t)$ describes the vehicle motion probability distribution, $p(x_{t-1})$ is the prior belief of the vehicle state, $p(y_t|x_t)$ is the likelihood function given in Equation 12, and α is a normalization constant.

3 Baseline TRN System with AUV-Based Maps

The map resolution studies performed in this paper are based on data collected from two sets of field trials performed in 2008 on the MBARI Dorado mapping AUV in Monterey Bay, California. The mapping vehicle, pictured in Figure 1, is a high-performance system utilized by MBARI primarily for generating bathymetry maps with up to 30cm vertical precision and less than one meter lateral resolution [16]. It is equipped with several sonar systems, including a 200kHz multibeam sonar, two sidescan sonars and a subbottom profiler. The navigation system consists of an integrated Kearfott INS and RDI 300 kHz DVL which provides an inertial drift rate of 0.05% of distance traveled, provided the DVL maintains bottom lock throughout the mission [17].

The terrain navigation algorithm described in Section 2 was implemented using the DVL sonar measurements from the vehicle's navigation system for terrain correlations. For these trials, 1m resolution DEM maps were used, previously generated by the mapping AUV. Utilizing these high-resolution maps in combination with the

Figure 1: Picture of retrieval of the MBARI Dorado mapping AUV. ©MBARI.

mapping AUV's high-performance navigation allows for the creation of performance baselines for the described TRN system, necessary for the performance studies in Section 4. The precise navigation system is particularly important for the presented studies as it allows for separation of performance effects due to sensor accuracy and those purely due to terrain map accuracy. For these field trials, both the resulting TRN estimation bias and variance are used as performance benchmarks for the analysis in Section 4 over coarser map resolutions.

On both missions, the TRN filter was run in real-time on-board the vehicle at an update rate of 0.1Hz, resulting in filter updates every 15 meters. This lower rate was chosen to minimize the load on the CPU, a LiPPERT Cool SpaceRunner 2 with 300MHz processor speed and 128MB SDRAM. Even at this lower rate, however, the terrain navigation algorithm successfully converged for both field trials.

The first set of trials was performed in July, 2008 at Soquel Canyon in Monterey Bay. Figure 2 shows the DEM map along with both the inertial estimate and terrain navigation estimate of the vehicle trajectory. The trajectory was chosen along this narrow strip of the mapped canyon in order to ensure that the vehicle would start at a shallow enough depth to maintain DVL lock, and thus precise navigation, for the duration of the mission. The 90% confidence ellipsoids of the TRN estimate are also shown. Figure 3 shows the filter estimates for North, East and Depth versus distance traveled. The TRN filter converges after approximately 30 measurements, or 400 meters.

The second set of trials was performed in August, 2008 at Portuguese Ledge in Monterey Bay, the same site as previous trials described in [8]. The DEM map, inertial estimate and TRN estimate of vehicle trajectory are shown in Figure 4. This vehicle route was selected to maximize the variability of the terrain under the vehicle path, enabling faster estimator convergence than was
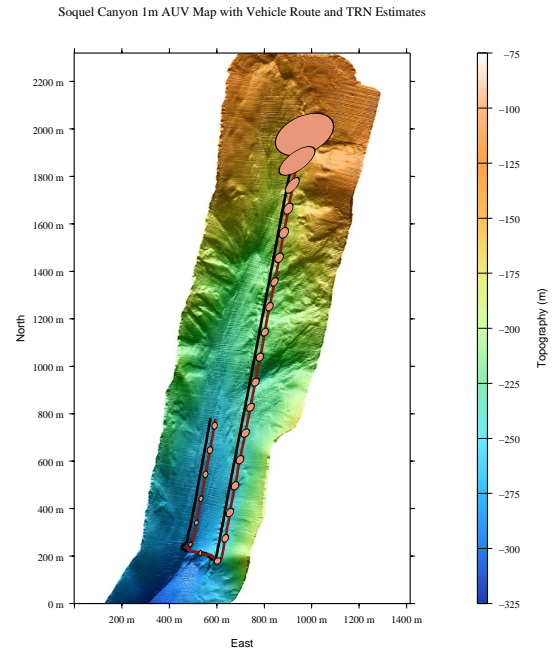

Figure 2: Soquel Canyon high resolution (1m) map with both Inertial and TRN estimated vehicle tracks. 90% confidence ellipses are shown around the TRN estimate. Figure generated using MB-System©.
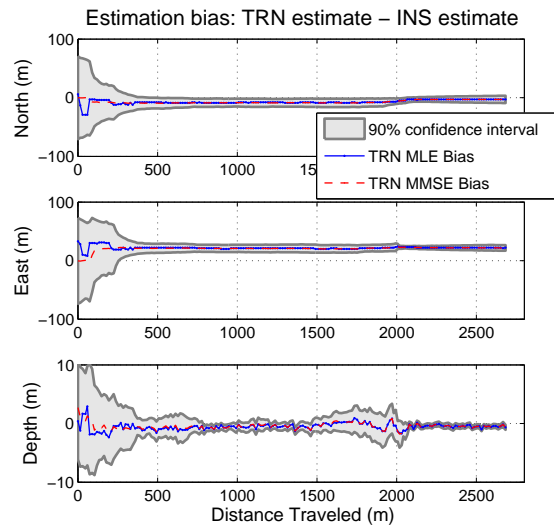

Figure 3: TRN estimator results in North, East and Depth for the Soquel Canyon field trial data.

achieved in the prior trials at this site. The vehicle was able to acquire DVL lock for the entire mission due to the shallowness of this site, ensuring high-performance inertial navigation. The terrain navigation estimates versus distance traveled are shown in Figure 5. The estimator converges rapidly upon reaching the rougher part of the terrain, after just 20 measurements or 300 meters.
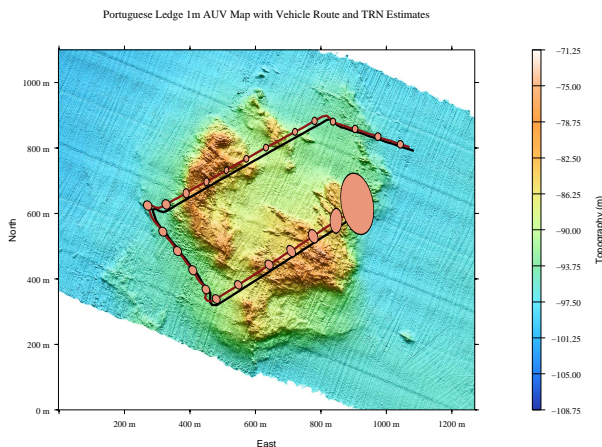

Figure 4: Portuguese Ledge high resolution (1m) map with both Inertial and TRN estimated vehicle tracks. 90% confidence ellipses are shown around the TRN estimate. Figure generated using MB-System©.

Table 1 shows the final TRN estimate variance and bias from inertial for both field trials.

Table 1: TRN Estimates for Field Trials using 1m Resolution Maps

		North(m)	East(m)	Depth(m)
Soquel	Bias	-2.94	21.6	-0.65
Canyon	σ	2.48	1.9	0.16
Portuguese	Bias	11.15	-12.54	0.51
Ledge	σ	3.22	2.74	0.05

Since the terrain navigation filter provides a terrain-relative position estimate, the resulting bias is a combination of both inertial navigation error and map geo-registration error. The inertial drift component of the navigation error is expected to be small for these trials due to the high-precision INS unit, at most 1-2m for both trials. Surface initialization errors in the inertial navigation may also exist, however, which may also contribute to the observed bias. The expected magnitude of the geo-registration error was assessed by using a 2D correlation technique to register the coarse
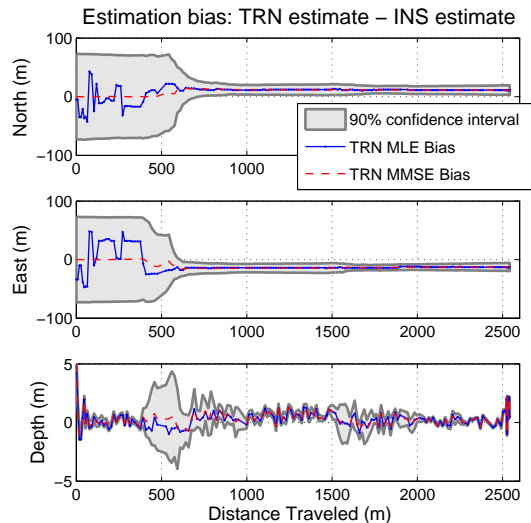

Figure 5: TRN estimator results in North, East and Depth for the Portuguese Ledge field trial data.

ship-based maps from Section 5 with the high-resolution AUV-based maps for both sites. The resulting expected geo-referencing errors are shown in Table 2.

Table 2: Estimated Geo-Referencing Errors for AUV-Based DEMs

	North(m)	East(m)
Soquel Canyon	1.1	11.3
Portuguese Ledge	17.4	-13.3

Given this combination of expected error sources, the resulting magnitudes of the TRN estimation biases in Table 1 are very reasonable.

4 Map Resolution Performance Studies

Utilizing coarser terrain maps for terrain relative navigation is expected to degrade the overall achievable accuracy, with the degree of performance reduction depending on several factors including both terrain variability and vehicle trajectory. In order to evaluate this performance trade-off, both analytical and empirical performance studies were completed using the recorded data from the field trials discussed in the previous section over a set of generated coarse terrain maps.

The coarse maps used in these studies were generated using the same processed multibeam sonar soundings used to generate the 1m resolution AUV maps utilized

in the online field trials. The open-source software MB-System©was used to generate lower resolution maps from this sonar data. The employed gridding function computes each DEM grid cell value by a Gaussian-weighted average of the sonar soundings falling within that cell. This map generation method was used because it is the same method employed to generate the ship-based bathymetry maps, thereby resulting in more comparable DEMs than simple sub-sampling or regular averaging. For the following studies, the coarse maps were generated for both Portuguese Ledge and Soquel Canyon at resolutions of 2m, 5m, 10m, 15m, 20m, 25m and 30m.

4.1 Empirical Performance Studies

In order to assess TRN performance with decreased map resolution, experimental tests were performed first by running the terrain navigation filter over the generated low-resolution DEMs for both field data sets. Figure 6 shows the resulting filter performance for the Soquel Canyon data, shown as root mean squared error (RMSE) for both North and East. The RMSE is further decomposed into bias and variance. The bias is computed as the deviation in the TRN estimate from the nominal estimates over 1m resolution maps, shown in Table 1. Figure 7 shows the equivalent results for the Portuguese Ledge data set.
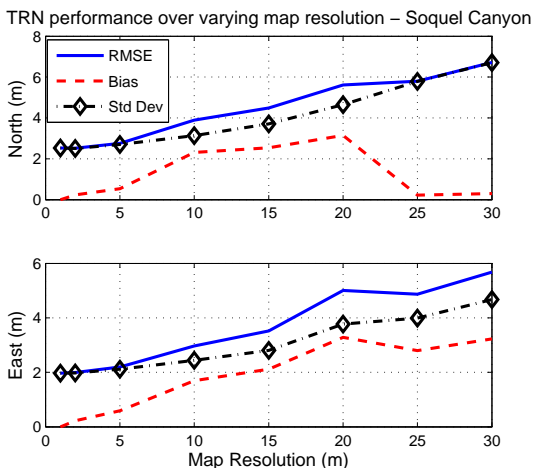

Figure 6: Root mean square error of the final TRN estimate for varying map resolution at Soquel Canyon. Results are shown as total RMSE as well as the component bias and standard deviation for both North and East.

The results from these experiments show that the increase in RMSE of the TRN estimator with decreased map resolution occurs gradually. Furthermore, despite differences in the relative decomposition of bias and
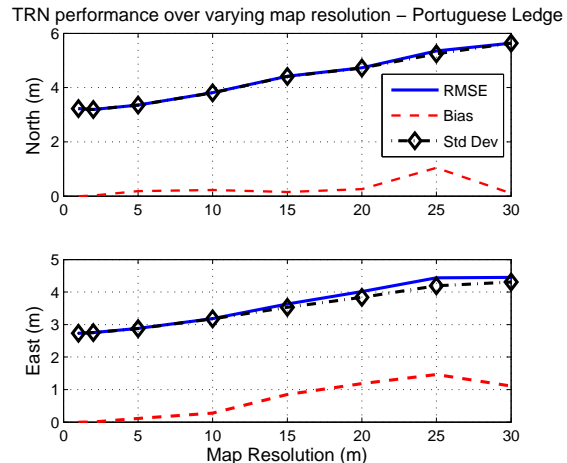

Figure 7: Root mean square error of the final TRN estimate for varying map resolution at Portuguese Ledge. Results are shown as total RMSE as well as the component bias and standard deviation for both North and East.

variance for the two data sets, the overall rate of performance degradation is highly comparable. In order to understand the underlying cause of these observed similarities and differences between the two terrains, analytical studies were performed for both data sets, which are discussed in the following section.

4.2 Analytical Performance Studies

A posterior Cramér-Rao Lower Bound (PCRLB) analysis was utilized to provide an analytical bound on TRN performance over the generated low-resolution maps. The PCRLB is an extension of the common Cramér-Rao Lower Bound (CRLB), which provides a lower bound on the mean square error of any unbiased estimator for time-invariant systems. The CRLB is defined as the inverse of the Fisher Information matrix, J, computed directly from the measurement probability distribution (e.g. [18]):

$$CRLB = J^{-1} \leq E\left[[\hat{x} - x][\hat{x} - x]^T\right] \quad (16)$$

where

$$J = -E\left[\frac{\partial^2 \ln p(y|x)}{\partial x_i \partial x_j}\right]. \quad (17)$$

For dynamic systems where the state exhibits uncertain change, a posterior Cramér-Rao bound can be found by utilizing the full Fisher information matrix over the joint probability distribution of the measurement and state:

$$\bar{J}_n = -E\left[\frac{\partial^2 \ln p(y_n, x_n)}{\partial x_i \partial x_j}\right]. \quad (18)$$

While applicable to many systems, the PCRLB is particularly powerful as a performance assessment tool for non-linear filters, such as the point mass filter used in this paper. Tichavksy et al. [19] developed a very useful formulation of this bound specifically for discrete-time nonlinear filters. The authors show that $\bar{J}_n$ can be calculated via the Ricatti-like recursion shown in Equation 19

$$\bar{J}_{n+1} = D_n^{22} - D_n^{21}(\bar{J}_n + D_n^{11})^{-1}D_n^{12} \quad (19)$$

where

$$
\begin{aligned}
D_n^{11} &= E\left[-\frac{\partial^2}{\partial x_n^2}\log p(x_{n+1}|x_n)\right] \\
D_n^{12} &= E\left[-\frac{\partial^2}{\partial x_n \partial x_{n+1}}\log p(x_{n+1}|x_n)\right] \\
D_n^{21} &= [D_n^{12}]^T \\
D_n^{22} &= E\left[-\frac{\partial^2}{\partial x_{n+1}^2}\log p(x_{n+1}|x_n)\right] \\
&\quad + E\left[-\frac{\partial^2}{\partial x_{n+1}^2}\log p(z_{n+1}|x_{n+1})\right] \\
&= D_{n1}^{22} + D_{n2}^{22}. \quad (20)
\end{aligned}
$$

For systems with additive Gaussian process and measurement noise, as with the TRN system, Equation 19 simplifies significantly with $D_n^{11} = D_n^{12} = D_{n1}^{22} = \Sigma_{r,n}^{-1}$ and $D_{n2}^{22} = J$, the Fisher Information matrix for the standard CRLB. In this simplified case, the PCRLB is the covariance of the Extended Kalman Filter.

Both versions of the Cramér-Rao bound have been successfully applied to performance assessment in terrain navigation systems, with the CRLB being used for batch TRN systems [3] and the PCRLB for non-linear Bayesian TRN implementations [5], [20]. The PRCLB for the current TRN filter implementation described in Section 2 is identical to that derived by Bergman [20], with a modified J term for the likelihood function described in Equation 12. Using the Matrix Inversion lemma to rearrange Equation 19, the resulting PCRLB for the employed TRN filter is given by:

$$PCRLB_n = \bar{J}_n^{-1} \le E\left[[\hat{x}_n - x_n][\hat{x}_n - x_n]^T\right] \quad (21)$$

where

$$\bar{J}_{n+1} = H_{n+1}^T \Pi_{n+1}^T \Sigma_{w,n}^{-1}\Pi_{n+1}H_{n+1} + (\bar{J}_n^{-1}+\Sigma_{r,n})^{-1} \quad (22)$$

and $H_n = \nabla_x \hat{h}(x_n)$ is the terrain gradient matrix for the current measurement. Note that the terrain gradients in H_n are the gradients seen by the estimation filter, *not* the true gradients of the physical terrain. Thus this matrix is determined by both the utilized DEM map and the employed interpolation method.

Figure 8 shows the result of applying the PCRLB in Equation 22 to the Soquel Canyon data set over the generated coarser maps. The root mean square error from the empirical studies is shown as well for comparison. The corresponding results are shown in Figure 9 for the Portuguese Ledge field data.
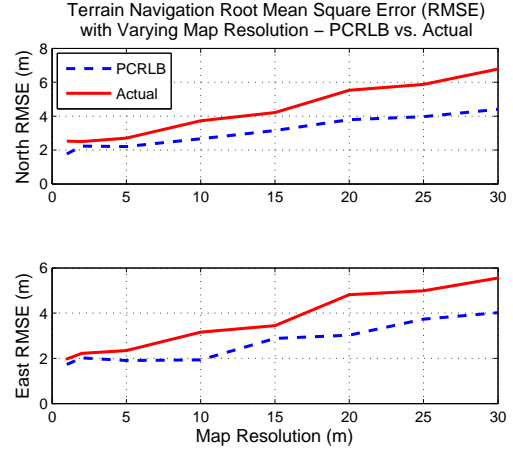

Figure 8: Posterior Cramer-Rao Lower Bound for the Soquel Canyon data set shown along with the experimentally determined RMSE.

For both data sets, the estimator performance trend follows that of the PCRLB. For Soquel Canyon, the gap between estimator RMSE and the PCRLB is noticeably larger than that for Portuguese Ledge, a result of the larger biases observed in the estimator for coarser map resolutions.
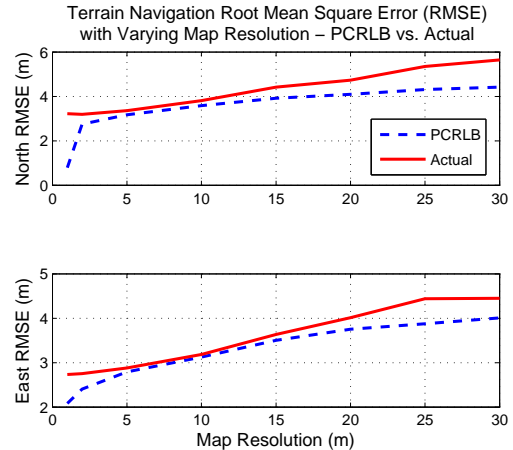

Figure 9: Posterior Cramer-Rao Lower Bound for the Portuguese Ledge data set shown along with the experimentally determined RMSE.

While the PCRLB is not an exact predictor of esti-

mator performance (i.e., the performance bound is not met for this data), it can still provide a meaningful tool for assessing the sources of performance variability for these different terrains. From Equation 22, reduced TRN estimator performance can be attributed to two primary factors: (1) decreases in H, corresponding to reduced variability in the represented terrain gradients, and (2) increases in Σ_w, corresponding to decreased accuracy of individual DEM points. Thus to better understand the performance similarities and differences noted in Section 4.1, comparisons of these two factors were made for the two sets of field trials.

Figure 10 shows a comparison of terrain gradient statistics for the Portuguese Ledge and Soquel Canyon maps for varying resolutions. The terrain slopes used for these statistics were computed for the section of terrain along the vehicle path. For both terrains, the slope magnitude and variability is seen to decrease primarily from 1m to 5m, and then level off for coarser map resolutions. This leveling behavior mimics the concave, gradual incline of the PCRLB curves seen in Figures 8 and 9.
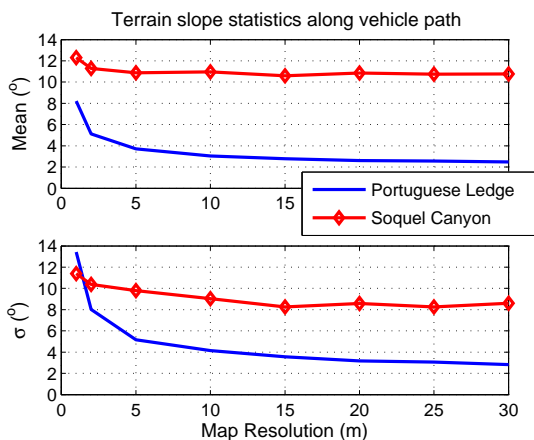

Figure 10: Comparison of terrain slope statistics along vehicle path for Soquel Canyon and Portuguese Ledge.

Figure 10 further illustrates that the Soquel Canyon terrain maps exhibit both significantly larger overall slope variability and slope magnitude than the Portuguese Ledge maps for nearly all map resolutions. This characteristic alone suggests higher performance TRN for the Soquel Canyon terrain. However, as noted earlier, the performance is also effected by the DEM accuracy.

DEM accuracy is represented in Σ_w by the σ_v^2 term, defined in Equation 8. The magnitude of σ_v^2 depends on both the accuracy of the DEM generation process and the underlying variability in the terrain, represented by the variogram, $\gamma(s)$. Indeed, the RMSE of interpolated DEM values has been shown to be a direct function of the variogram [11]. Thus for the same quality underlying DEM measurements, the accuracy of interpolated

DEM elevations will be larger for terrains with larger variograms.

Figure 11 shows the variograms for the Soquel Canyon and Portuguese Ledge terrains over the range of map resolutions considered in these studies. The variograms were computed using the fractal model described in Equation 8.
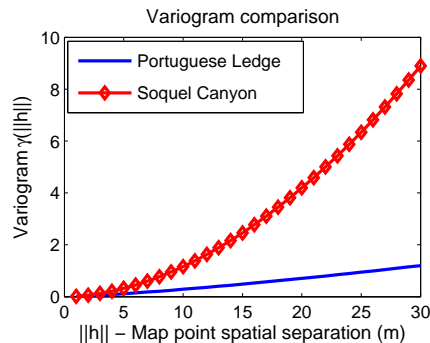

Figure 11: Comparison of Variograms

Note that the variogram for Soquel Canyon increases significantly with lag distance, compared to a much more gradual incline for Portuguese Ledge. As a result, the Soquel Canyon data is expected to exhibit noticeably reduced DEM accuracy at coarser resolutions. This reduced map accuracy combined with large slope variability noted in Figure 10 makes the Soquel Canyon terrain much more susceptible to terrain model errors than the Portuguese Ledge data set, resulting in the larger observed estimator biases. In addition, however, the large terrain gradients observed for the Soquel Canyon data balance the reduced DEM accuracy in terms of the estimator variance, predicted by the PCRLB.

TRN performance reduction with coarser maps can thus be ascribed to the decreased ability of the resulting terrain model to accurately represent both the true slope variability and elevation. For flatter terrains, the performance reduction will primarily result from reduced DEM slope variability. Conversely, TRN over terrains with larger slope and elevation variability will be effected primarily by reduced DEM elevation accuracy. Thus in many physical terrains, the effect of H and Σ_w in the PCLRB are expected to counter-balance, resulting in comparable TRN performance reductions regardless of the underlying terrain.

5   TRN with Ship-Based Maps

While the studies in the previous section are insightful, it is important to assess how well this analysis on artificially coarse maps matches with truly coarse DEM maps

generated from ship-based bathymetry. As noted earlier, ship-based bathymetry is available for a large section of Monterey Bay, including the sites for both of the presented field trials. Using this ship-based multibeam sonar data, 20m resolution DEM maps were generated for both Portuguese Ledge and Soquel Canyon using the same MB-System©gridding method as described in Section 4.

Figures 12 and 13 show the DEM maps for Soquel Canyon and Portuguese Ledge, respectively, overlaid with the terrain navigation estimated vehicle tracks and 90% confidence ellipses. The corresponding final estimation bias and variance are shown in Table 3, along with the PCRLB performance bound computed in Section 4.2 for a 20m resolution map.

Figure 13: TRN estimator results for Portuguese Ledge field trials, using ship-based, 20m resolution bathymetry map. Figure generated using MB-System©.

Table 3: TRN Estimates for Field Trials using 20m Resolution Ship-Based Maps

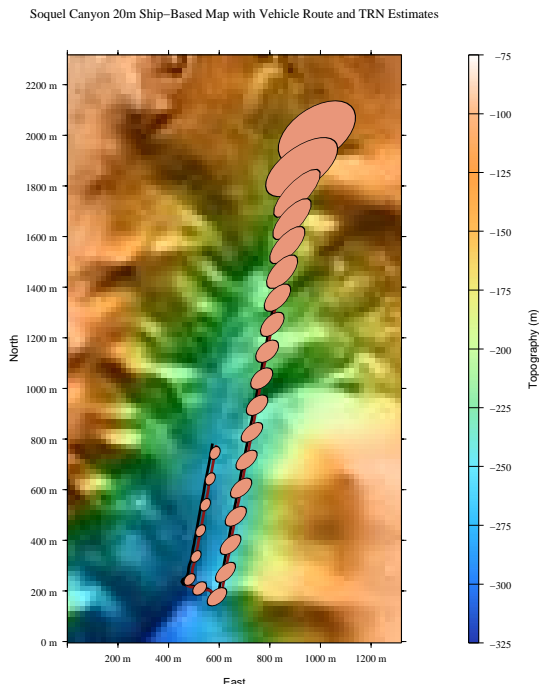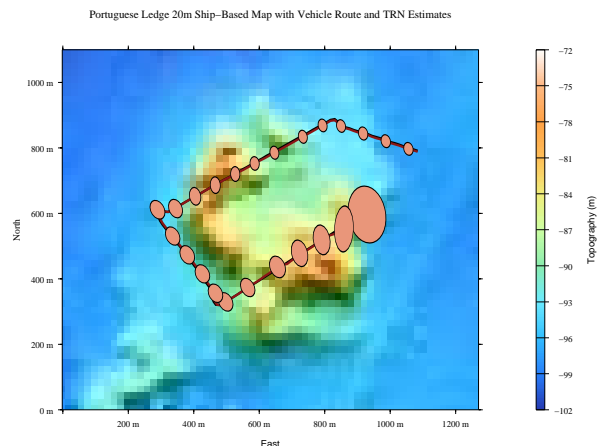|		North(m)	East(m)	Depth(m)
Soquel Canyon	Bias	-7.31	14.86	0.31
	σ	4.53	3.64	0.23
	RMSE	8.6	15.3	0.38
	$\sqrt{PCRLB}$	3.79	3.03	–
Portuguese Ledge	Bias	-3.15	0.03	0.3
	σ	5.16	3.91	0.03
	RMSE	6.05	3.91	0.3
	$\sqrt{PCRLB}$	4.09	3.75	–

Figure 12: TRN estimator results for Soquel Canyon field trials, using ship-based, 20m resolution bathymetry map. Figure generated using MB-System©.

Note that since these maps are generated from ships which can maintain gps lock during data acquisition, the contribution of the geo-referencing error to the resulting TRN bias is expected to be small. However, initialization errors in the inertial navigation are still plausible. In addition, TRN estimation bias on the order of a couple meters is expected simply due to the decreased map resolution, observed in Section 4.1.

For both of these data sets, the observed estimator variances are very comparable to the predicted estima-

tion performance provided by the PCRLB. In addition, the resulting estimation bias from the inertial navigation is reasonable given the expected bias sources noted above. This similarity of predicted and actual performance indicates that the presented map resolution studies in Section 4 are realistic predictions of TRN performance on actual coarse DEMs.

6   Conclusions

The presented performance studies in this paper indicate that, while TRN performance does degrade with decreased map resolution as expected, this reduction occurs gradually. Moving from a 1m to a 30m resolution map was observed to decrease estimator accuracy from $\sim 2m$ to $\sim 6m$ RMSE. A posterior Cramér-Rao bound

analysis demonstrated that the observed degree of performance reduction is primarily related to two counteracting characteristics in the underlying terrain: variability in terrain slope and elevation.

For a fairly flat terrain, reduction in map resolution significantly decreased the overall terrain gradient distribution, resulting in reduced achievable TRN performance. However, this reduction was counteracted by the terrain's small elevation variability, resulting in minimal DEM inaccuracies at coarser resolutions. In a more steeply sloped terrain, these effects were found to be opposite. It is expected that these two characteristics will naturally compete in any terrain surface, resulting in comparable performance reduction rates for many natural terrain surfaces.

The results in this paper thus suggest that readily available ship-based bathymetry can provide sufficient terrain information to achieve TRN accuracies less than the map resolution. While the use of high-resolution AUV-based maps will provide improved performance when available, such maps are not crucial to successful TRN and may be unnecessary for many applications.

Acknowledgments

References

[1] J. P. Golden, "Terrain countour matching(tercom): a cruise missile guidance aid," *SPIE*, vol. 238, pp. 10–18, 1980.

[2] B. Jalving and O. Mandt, M. Hagen, "Terrain referenced navigation of auvs and submarines using multibeam echo sounders," in *UDT '04*. Nice, France: Norwegian Defence Res. Establ, June 2004.

[3] I. Nygren, "Terrain navigation for underwater vehicles," Ph.D. dissertation, Royal Institute of Technology, Stockholm, Sweden, 2005.

[4] K. B. Anonsen and O. Hallingstad, "Terrain aided underwater navigation using point mass and particle filters," in *IEEE PLANS*, April 2006, pp. 1027–1035.

[5] R. Karlsson and F. Gustafsson, "Bayesian surface and underwater navigation," *IEEE Transactions on Signal Processing*, vol. 54, no. 11, p. 4204, 2006.

[6] J. Carlstrom, "Results from sea trials of the swedish auv62fs terrain navigation system," in *UUST '07: Unmanned Untethered Submersible Technology*. Saab Underwater Systems, 2007.

[7] A. Sarma, "Maximum likelihood estimates and cramer-rao bounds for map-matching based self-localization," in *OCEANS '07*, October 2007.

[8] D. Meduna, S. Rock, and R. McEwen, "Low-cost terrain relative navigation for long-range auvs," in *OCEANS '08: Oceans, Poles and Climate: Technological Challenges*, Quebec City, Quebec, September 2008.

[9] N. Fairfield and D. Wettergreen, "Active localization on the ocean floor with multibeam sonar," in *OCEANS '08: Oceans, Poles and Climate: Technological Challenges*, Quebec City, Quebec, September 2008.

[10] L. Stutters, H. Liu, C. Tiltman, and D. Brown, "Navigation technologies for autonomous underwater vehicles," *IEEE Transactions on Systems, Man, and Cybernetics, Part C: Applications and Reviews*, vol. 38, no. 4, pp. 581–589, 2008.

[11] W.G.Rees, "The accuracy of digital elevation models interpolated to higher resolutions," *International Journal of Remote Sensing*, vol. 21, no. 1, pp. 7–20, 2000.

[12] J. Li, G. Taylor, and D. Kidner, "Accuracy and reliability of map-matched gps coordinates: the dependence on terrain model resolution and interpolation algorithm," *Computers and Geosciences*, vol. 31, pp. 241–251, 2005.

[13] G. Matheron, "Principles of geostatistics," *Economic Geology*, vol. 58, no. 8, pp. 1246–1266, 1963.

[14] J. Zhang and M. Goodchild, *Uncertainty in Geographical Information*. CRC, 2002.

[15] B. Mandelbrot, *The Fractal Geometry of Nature*. Wh Freeman, 1982.

[16] R. Henthorn, D. Caress, H. Thomas, R. Mcewen, W. Kirkwood, C. Paull, and R. Keaten, "High-resolution multibeam and subbottom surveys of submarine canyons, deep-sea fan channels, and gas seeps using the mbari mapping auv," in *OCEANS*. MBARI, Sept. 2006, pp. 1–6.

[17] W. J. Alameda, "Seadevil a totally integrated inertial navigation system (ins) solution," in *Underwater Intervention Symposium*, 2002.

[18] S. M. Kay, *Fundamentals of Statistical Signal Processing*.   Prentice Hall PTR, 1993.

[19] P. Tichavsky, C. Muravchik, and A. Nehorai, "Posterior cramer-rao bounds for discrete-time nonlinear filtering," *IEEE Transactions on Signal Processing*, vol. 46, pp. 1386–1396, May 1998.

[20] N. Bergman, "Recursive bayesian estimation: Navigation and tracking applications," Ph.D. dissertation, Linkoping University, Linkoping, Sweden, 1999.